

# Forward-backward multiplicity correlations of target fragments in nucleus-emulsion collisions at a few hundred MeV/u<sup>\*</sup>

ZHANG Dong-Hai(张东海)<sup>1)</sup> CHEN Yan-Ling(陈艳玲) WANG Guo-Rong(王国蓉)  
 LI Wang-Dong(李王东) WANG Qing(王青) YAO Ji-Jie(姚继杰) ZHOU Jian-Guo(周建国)  
 LI Rong(李蓉) LI Jun-Sheng(李俊生) LI Hui-Ling(李惠玲)

Institute of Modern Physics, Shanxi Normal University, Linfen 041004, China

**Abstract:** The forward-backward multiplicity and correlations of a target evaporated fragment (black track particle) and target recoiled proton (grey track particle) emitted from 150 A MeV <sup>4</sup>He, 290 A MeV <sup>12</sup>C, 400 A MeV <sup>12</sup>C, 400 A MeV <sup>20</sup>Ne and 500 A MeV <sup>56</sup>Fe induced different types of nuclear emulsion target interactions are investigated. It is found that the forward and backward averaged multiplicity of a grey, black and heavily ionized track particle increases with the increase of the target size. The averaged multiplicity of a forward black track particle, backward black track particle, and backward grey track particle do not depend on the projectile size and energy, but the averaged multiplicity of a forward grey track particle increases with an increase of projectile size and energy. The backward grey track particle multiplicity distribution follows an exponential decay law and the decay constant decreases with an increase of target size. The backward-forward multiplicity correlations follow linear law which is independent of the projectile size and energy, and the saturation effect is observed in some heavy target data sets.

**Key words:** heavy-ion collisions, target fragmentation, multiplicity, correlation, nuclear emulsion

**PACS:** 25.70.-z, 25.70.Mn, 25.70.Pq **DOI:** 10.1088/1674-1137/39/1/014001

## 1 Introduction

The study of the production of backward particles in hadron-nucleus and nucleus-nucleus interactions at high energies has received considerable experimental and theoretical attention because the fact that the backward emission of relativistic particles in high energy hadron-nucleon collisions is kinematically restricted. The backward emission of protons and pions in hadron-nucleus [1–7] and nucleus-nucleus [8–18] at relativistic energies have been investigated exclusively. It is found that the backward proton production was attributed to the absorption of secondary pions by a nucleon pair in the target nucleus, and the backward pions production shown to be consistent with the cumulative effect [19]. The emission of target evaporated fragments is isotropic in the rest system of a target nucleus according to the cascade evaporation model [20], but attributed to the electromagnetic field from projectile, the emission of target evaporated fragments is close to  $\theta \approx 90^\circ$  symmetric and the multiplicity in a forward hemisphere is greater than that in a backward hemisphere. There is no reasonable theoretical model to explain the salient features of forward-

backward multiplicity correlations. Little attention has been paid to the study of the particle production in a backward hemisphere and forward-backward multiplicity correlations in nucleus-nucleus collisions at intermediate and high energies (a few hundreds MeV/u).

According to the participant-spectator model [21] of the high energy nucleus-nucleus collisions, the projectile and target sweep out cylindrically cut-through each other. The overlapping region of nuclear volumes is called the participant region, where multiple production of new particles occurs and the nuclear matter breaks up into nucleons. The remaining parts of nuclei which do not participate in the disintegration process are called the spectators of the projectile and target nuclei. In a central collision the projectile drills a cylindrical hole through the target nucleus, striking every nucleon in its path. Some of the struck nucleons will penetrate into the spectator part whereas some will escape through the hole. It is assumed that effectively only those nucleons that are originating from the surface region of the cylinder penetrates the spectator and that these nucleons move away from the centre of the hole. In a peripheral or semi-central collision only a part of the cylindrical

Received 19 March 2014

<sup>\*</sup> Supported by National Science Foundation of China (11075100), Natural Science Foundation of Shanxi Province, China (2011011001-2) and Shanxi Provincial Foundation for Returned Overseas Chinese Scholars, China (2011-058)

1) E-mail: zhangdh@dns.sxnu.edu.cn

©2015 Chinese Physical Society and the Institute of High Energy Physics of the Chinese Academy of Sciences and the Institute of Modern Physics of the Chinese Academy of Sciences and IOP Publishing Ltd

hole is developed, and here the probability that a struck target nucleon will disappear without penetrating into the spectator increases with the decrease of the collision centrality. During this colliding process, a fraction of the available energy is transferred to the spectator parts of colliding nuclei, leaving those nuclear remnants in an excited state. After this stage, the de-excitation of the nuclear remnants take place and the target and projectile fragments are formed. In general, this reaction mechanism is also reasonable for the intermediate and high energy, but the production of new particles in the participant region is highly suppressed because of the limited reaction energy.

In this paper the forward-backward multiplicity and correlations of a target evaporated fragment and target recoiled proton of 150 A MeV  $^4\text{He}$ , 290 A MeV  $^{12}\text{C}$ , 400 A MeV  $^{12}\text{C}$ , 400 A MeV  $^{20}\text{Ne}$  and 500 A MeV  $^{56}\text{Fe}$  induced different types of nuclear emulsion target interactions are investigated. We want to find out the general characteristics of the particle production in the backward hemisphere and forward-backward multiplicity correlations in nucleus-nucleus collisions at intermediate and high energies.

## 2 Experimental details

Five stacks of nuclear emulsion made by the Institute of Modern Physics, Shanxi Normal University, China, are used in the present investigation. The emulsion stacks were exposed horizontally at HIMAC, NIRS, Japan. The beams were 150 A MeV  $^4\text{He}$ , 290 A MeV  $^{12}\text{C}$ , 400 A MeV  $^{12}\text{C}$ , 400 A MeV  $^{20}\text{Ne}$  and 500 A MeV  $^{56}\text{Fe}$  respectively, and the flux was 3000 ions/cm<sup>2</sup>. BA2000 and XSJ-2 microscopes with a 100 $\times$  oil immersion objective and 10 $\times$  ocular lenses were used to scan the plates. The tracks were picked up at a distance of 5 mm from the edge of the plates and were carefully followed until they either interacted with emulsion nuclei or escaped from the plates. Interactions which were within 30  $\mu\text{m}$  from the top or bottom surface of the emulsion plates were not considered for final analysis. All the primary tracks were followed back to ensure that the events chosen did not include interactions from the secondary tracks of other interactions. When they were observed to do so the corresponding events were removed from the sample.

In each interaction all of the secondaries were recorded which included shower particles, target recoiled protons, target evaporated fragments and projectile fragments. According to the emulsion terminology [20], the particles emitted from high energy nucleus-emulsion interactions are classified as follows:

(a) Black track particles ( $N_b$ ). They are target evaporated fragments with ionization  $I > 9I_0$ ,  $I_0$  being the minimum ionization of a single charged particle. The range

of the black particle in nuclear emulsion is  $R < 3$  mm, velocity is  $v < 0.3c$ , and energy is  $E < 26$  MeV. The multiplicity of the black track particle emitted in the forward (emission angle  $\theta \leq 90^\circ$ ) and backward hemisphere ( $\theta > 90^\circ$ ) is denoted as  $n_b^f$  and  $n_b^b$  respectively, and the total multiplicity is denoted as  $n_b$ .

(b) Grey track particles ( $N_g$ ). They are mostly recoil protons in the kinetic energy range  $26 \leq E \leq 375$  MeV and pions with kinetic energies  $12 \leq E \leq 56$  MeV. They have ionization  $1.4I_0 \leq I \leq 9I_0$ . Their ranges in emulsion are greater than 3 mm and have velocities within  $0.3c \leq v \leq 0.7c$ . The multiplicity of the grey track particle emitted in the forward and backward hemisphere is denoted as  $n_g^f$  and  $n_g^b$  respectively, and the total multiplicity is denoted as  $n_g$ .

The grey and black track particles together are called heavy ionizing particles ( $N_h$ ). The multiplicity of the heavy ionizing particle emitted in the forward and backward hemisphere is denoted as  $n_h^f$  and  $n_h^b$  respectively, and the total multiplicity is denoted as  $n_h$ .

(c) Shower particles ( $N_s$ ). They are produced single-charged relativistic particles having a velocity of  $v \geq 0.7c$ . Most of them belong to pions contaminated with small proportions of fast protons and K mesons. It should be mentioned that for nucleus-emulsion interactions at a few hundred MeV/u most of the shower particles are projectile protons not pions.

(d) The projectile fragments ( $N_f$ ) are a different class of tracks with constant ionization, long range, and a small emission angle.

The nuclear emulsion is composed of an homogeneous mixture of nuclei. The chemical composition of the nuclear emulsion is H, C, N, O, S, I, Br, and Ag, and the major composition is H, C, N, O, Br, and Ag. According to the value of  $n_h$  the interactions are divided into the following three groups.

Events with  $n_h \leq 1$  are due to interactions with the H target and peripheral interactions with CNO and AgBr targets.

Events with  $2 \leq n_h \leq 7$  are due to interactions with CNO targets and peripheral interactions with AgBr targets.

Events with  $n_h \geq 8$  definitely belong to interactions with AgBr targets.

## 3 Results and discussion

Figure 1 shows the multiplicity distribution of backward grey track particles in different types of 150 A MeV  $^4\text{He}$ , 290 A MeV  $^{12}\text{C}$ , 400 A MeV  $^{12}\text{C}$ , 400 A MeV  $^{20}\text{Ne}$  and 500 A MeV  $^{56}\text{Fe}$  induced nuclear emulsion interactions. It is found that the probability decreases with the increase of  $n_g^b$ , which can be well represented by an exponential decay law with the form of  $p(n_g^b) = a \exp(-\lambda n_g^b)$ .

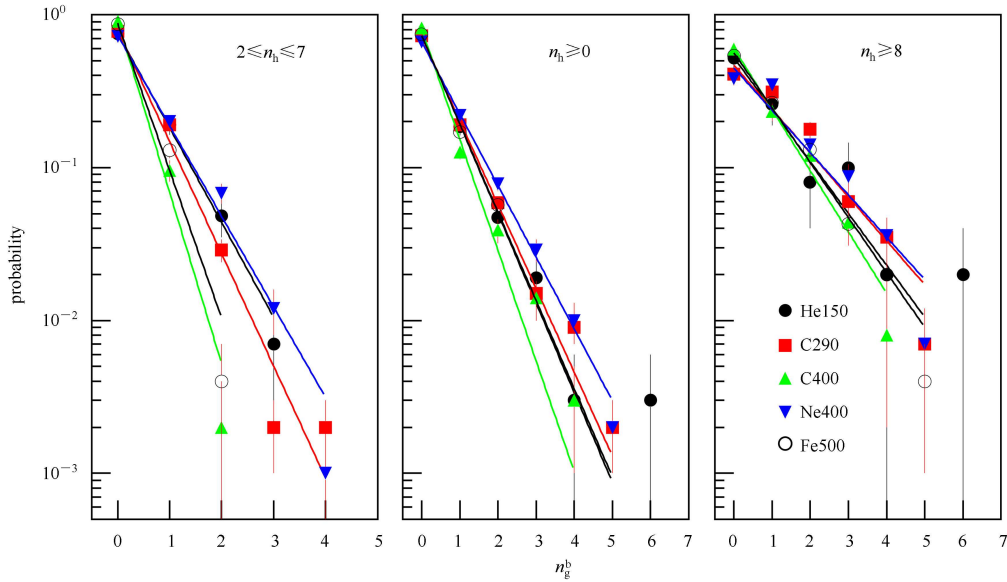


Fig. 1. (color online) Multiplicity distributions of a backward grey track particle in different types of interactions; the smooth curve is fitted by an exponential distribution.

The fitting parameters and event statistics ( $N_{ev}$ ) are presented in table 1. The decay constant  $\lambda$  decreases with the increase of target size, and no evident dependence of projectile size and energy is found in the present investigation.

Table 1. The exponential fitting parameters of  $n_g^b$  distribution in different types of nucleus-emulsion interactions.

type of interaction	$a$	$\lambda$	$N_{ev}$
150 A MeV $^4\text{He}$ -CNO	$0.761 \pm 0.051$	$1.428 \pm 0.094$	272
150 A MeV $^4\text{He}$ -Em	$0.737 \pm 0.044$	$1.348 \pm 0.081$	360
150 A MeV $^4\text{He}$ -AgBr	$0.521 \pm 0.094$	$0.781 \pm 0.147$	50
290 A MeV $^{12}\text{C}$ -CNO	$0.799 \pm 0.026$	$1.689 \pm 0.045$	1086
290 A MeV $^{12}\text{C}$ -Em	$0.715 \pm 0.019$	$1.264 \pm 0.035$	1850
290 A MeV $^{12}\text{C}$ -AgBr	$0.466 \pm 0.027$	$0.660 \pm 0.032$	432
400 A MeV $^{12}\text{C}$ -CNO	$0.911 \pm 0.045$	$2.583 \pm 0.136$	450
400 A MeV $^{12}\text{C}$ -Em	$0.802 \pm 0.032$	$1.667 \pm 0.082$	799
400 A MeV $^{12}\text{C}$ -AgBr	$0.601 \pm 0.045$	$0.921 \pm 0.064$	250
400 A MeV $^{20}\text{Ne}$ -CNO	$0.735 \pm 0.031$	$1.365 \pm 0.048$	676
400 A MeV $^{20}\text{Ne}$ -Em	$0.660 \pm 0.001$	$1.080 \pm 0.033$	1093
400 A MeV $^{20}\text{Ne}$ -AgBr	$0.447 \pm 0.032$	$0.637 \pm 0.038$	277
500 A MeV $^{56}\text{Fe}$ -CNO	$0.880 \pm 0.039$	$2.221 \pm 0.102$	540
500 A MeV $^{56}\text{Fe}$ -Em	$0.728 \pm 0.024$	$1.329 \pm 0.048$	1321
500 A MeV $^{56}\text{Fe}$ -AgBr	$0.561 \pm 0.028$	$0.826 \pm 0.035$	558

Table 2 presents the averaged forward and backward multiplicity of black, grey, and heavy ionizing track particles produced in 150 A MeV  $^4\text{He}$ , 290 A MeV  $^{12}\text{C}$ , 400 A MeV  $^{12}\text{C}$ , 400 A MeV  $^{20}\text{Ne}$  and 500 A MeV  $^{56}\text{Fe}$  induced different types of nuclear emulsion target interactions. It is found that the value of  $\langle n_b^f \rangle$ ,  $\langle n_b^b \rangle$  and  $\langle n_g^b \rangle$  increases with the target size, and which is independent of the projectile size and energy. The value of  $\langle n_g^f \rangle$  is also increased with the target size and independent of the projectile size and energy except for the case

of 500 A MeV  $^{56}\text{Fe}$ -emulsion interactions. The ratio of forward-backward multiplicity for the grey track particle ( $(F/B)_g$ ) decreases with the increase of target size, but for the black track particle it is independent of the target size. The forward-backward multiplicity ratio for the grey track particle is greater than that for the black track particle, which is reasonably consistent with the prediction of the cascade evaporation model.

Figure 2 shows the correlation between  $\langle n_b^b \rangle$ ,  $\langle n_g^f \rangle$  and  $n_b$  for 290 A MeV  $^{12}\text{C}$ , 400 A MeV  $^{12}\text{C}$ , 400 A MeV  $^{20}\text{Ne}$ , and 500 A MeV  $^{56}\text{Fe}$  induced different types of emulsion target interactions. It can be seen that for interactions with  $n_h \geq 8$ ,  $\langle n_g^f \rangle$  decreases with the increase of  $n_b$  first and then becomes saturated except for 500 A MeV  $^{56}\text{Fe}$ -AgBr interaction, where  $\langle n_g^f \rangle$  decreases first and then increases with the increase of  $n_b$ , and finally becomes saturated;  $\langle n_b^b \rangle$  decreases slowly with an increase of  $n_b$  except for 500 A MeV  $^{56}\text{Fe}$ -AgBr interaction where  $\langle n_b^b \rangle$  increases slowly with an increase of  $n_b$ . For interactions with  $2 \leq n_h \leq 7$ ,  $\langle n_g^f \rangle$  decreases with the increase of  $n_b$ ,  $\langle n_b^b \rangle$  almost remains constant with the increase of  $n_b$ . For all of the interactions ( $n_h \geq 0$ ),  $\langle n_g^b \rangle$  increases slowly with the increase of  $n_b$ , and  $\langle n_g^f \rangle$  increases first and then becomes saturated with the increase of  $n_b$ . The correlations can be represented by a linear relation of the formula:

$$\langle n_g^j \rangle = an_b + b \quad (1)$$

where j means forward hemisphere (f) and backward hemisphere (b) respectively. The fitted lines are shown in Fig. 2 and the fitting parameters are presented in Tables 3–5. Some of the fitting parameters are from the first a few data sets.

Table 2. The averaged forward and backward multiplicity and forward-backward multiplicity ratio of black, grey and heavily ionized track particles in nucleus-emulsion interactions.

type of interaction	$\langle n_b^b \rangle$	$\langle n_b^f \rangle$	$\langle n_g^b \rangle$	$\langle n_g^f \rangle$	$\langle n_h^b \rangle$	$\langle n_h^f \rangle$	$(F/B)_b$	$(F/B)_g$	$(F/B)_h$
150 A MeV $^4\text{He-H}$	$0.16 \pm 0.06$	$0.26 \pm 0.07$	$0.05 \pm 0.04$	$0.34 \pm 0.08$	$0.21 \pm 0.07$	$0.61 \pm 0.08$	$1.63 \pm 0.75$	$6.80 \pm 6.01$	$2.90 \pm 1.04$
150 A MeV $^4\text{He-CNO}$	$0.71 \pm 0.05$	$1.50 \pm 0.07$	$0.31 \pm 0.04$	$1.42 \pm 0.08$	$1.01 \pm 0.06$	$2.92 \pm 0.08$	$2.11 \pm 0.18$	$4.58 \pm 0.64$	$2.89 \pm 0.19$
150 A MeV $^4\text{He-Em}$	$0.89 \pm 0.06$	$1.74 \pm 0.09$	$0.37 \pm 0.04$	$1.62 \pm 0.09$	$1.25 \pm 0.07$	$3.36 \pm 0.13$	$1.96 \pm 0.17$	$4.38 \pm 0.53$	$2.69 \pm 0.18$
150 A MeV $^4\text{He-AgBr}$	$2.42 \pm 0.25$	$4.14 \pm 0.36$	$0.92 \pm 0.18$	$3.66 \pm 0.43$	$3.34 \pm 0.25$	$7.80 \pm 0.45$	$1.71 \pm 0.23$	$3.98 \pm 0.91$	$2.34 \pm 0.22$
290 A MeV $^{12}\text{C-H}$	$0.07 \pm 0.01$	$0.30 \pm 0.03$	$0.03 \pm 0.01$	$0.27 \pm 0.02$	$0.10 \pm 0.02$	$0.56 \pm 0.03$	$4.29 \pm 0.75$	$9.00 \pm 3.07$	$5.60 \pm 1.16$
290 A MeV $^{12}\text{C-CNO}$	$0.68 \pm 0.02$	$1.91 \pm 0.04$	$0.26 \pm 0.02$	$1.37 \pm 0.04$	$0.94 \pm 0.03$	$3.28 \pm 0.04$	$2.81 \pm 0.10$	$5.27 \pm 0.43$	$3.49 \pm 0.12$
290 A MeV $^{12}\text{C-Em}$	$0.94 \pm 0.03$	$2.43 \pm 0.05$	$0.40 \pm 0.02$	$1.69 \pm 0.04$	$1.34 \pm 0.04$	$4.12 \pm 0.08$	$2.59 \pm 0.10$	$4.23 \pm 0.23$	$3.07 \pm 0.11$
290 A MeV $^{12}\text{C-AgBr}$	$2.28 \pm 0.07$	$5.38 \pm 0.13$	$1.02 \pm 0.05$	$3.58 \pm 0.11$	$3.30 \pm 0.08$	$8.96 \pm 0.15$	$2.36 \pm 0.09$	$3.51 \pm 0.20$	$2.72 \pm 0.08$
400 A MeV $^{12}\text{C-H}$	$0.08 \pm 0.03$	$0.16 \pm 0.04$	$0.00 \pm 0.00$	$0.31 \pm 0.05$	$0.08 \pm 0.03$	$0.47 \pm 0.05$	$2.00 \pm 0.90$		$5.88 \pm 2.29$
400 A MeV $^{12}\text{C-CNO}$	$0.98 \pm 0.04$	$1.95 \pm 0.06$	$0.10 \pm 0.01$	$1.36 \pm 0.06$	$1.08 \pm 0.05$	$3.31 \pm 0.07$	$1.99 \pm 0.10$	$13.60 \pm 1.49$	$3.06 \pm 0.16$
400 A MeV $^{12}\text{C-Em}$	$1.53 \pm 0.06$	$3.09 \pm 0.11$	$0.26 \pm 0.02$	$1.85 \pm 0.06$	$1.78 \pm 0.07$	$4.94 \pm 0.14$	$2.02 \pm 0.11$	$7.12 \pm 0.59$	$2.78 \pm 0.13$
400 A MeV $^{12}\text{C-AgBr}$	$3.08 \pm 0.12$	$6.31 \pm 0.21$	$0.64 \pm 0.06$	$3.32 \pm 0.13$	$3.72 \pm 0.13$	$9.63 \pm 0.24$	$2.05 \pm 0.10$	$5.19 \pm 0.53$	$2.59 \pm 0.11$
400 A MeV $^{20}\text{Ne-H}$	$0.20 \pm 0.03$	$0.34 \pm 0.04$	$0.06 \pm 0.02$	$0.07 \pm 0.02$	$0.26 \pm 0.04$	$0.41 \pm 0.04$	$1.70 \pm 0.32$	$1.17 \pm 0.51$	$1.58 \pm 0.29$
400 A MeV $^{20}\text{Ne-CNO}$	$0.92 \pm 0.04$	$1.63 \pm 0.05$	$0.38 \pm 0.03$	$0.90 \pm 0.04$	$1.30 \pm 0.04$	$2.53 \pm 0.05$	$1.77 \pm 0.09$	$2.37 \pm 0.21$	$1.95 \pm 0.07$
400 A MeV $^{20}\text{Ne-Em}$	$1.26 \pm 0.04$	$2.35 \pm 0.07$	$0.51 \pm 0.03$	$1.18 \pm 0.04$	$1.77 \pm 0.05$	$3.54 \pm 0.09$	$1.87 \pm 0.08$	$2.31 \pm 0.16$	$2.00 \pm 0.08$
400 A MeV $^{20}\text{Ne-AgBr}$	$2.62 \pm 0.09$	$5.12 \pm 0.16$	$1.07 \pm 0.07$	$2.44 \pm 0.11$	$3.69 \pm 0.10$	$7.56 \pm 0.17$	$1.95 \pm 0.09$	$2.28 \pm 0.18$	$2.05 \pm 0.07$
500 A MeV $^{56}\text{Fe-H}$	$0.12 \pm 0.02$	$0.32 \pm 0.03$	$0.02 \pm 0.01$	$0.30 \pm 0.03$	$0.14 \pm 0.02$	$0.62 \pm 0.03$	$2.67 \pm 0.51$	$15.00 \pm 7.65$	$4.43 \pm 0.67$
500 A MeV $^{56}\text{Fe-CNO}$	$0.69 \pm 0.03$	$1.38 \pm 0.05$	$0.14 \pm 0.02$	$2.33 \pm 0.07$	$0.83 \pm 0.04$	$3.72 \pm 0.07$	$2.00 \pm 0.11$	$16.64 \pm 2.43$	$4.48 \pm 0.23$
500 A MeV $^{56}\text{Fe-Em}$	$1.24 \pm 0.04$	$2.87 \pm 0.09$	$0.38 \pm 0.02$	$4.86 \pm 0.15$	$1.61 \pm 0.05$	$7.73 \pm 0.22$	$2.31 \pm 0.10$	$12.79 \pm 0.78$	$4.80 \pm 0.20$
500 A MeV $^{56}\text{Fe-AgBr}$	$2.21 \pm 0.07$	$5.32 \pm 0.15$	$0.75 \pm 0.04$	$9.13 \pm 0.25$	$2.96 \pm 0.09$	$14.46 \pm 0.33$	$2.41 \pm 0.10$	$12.17 \pm 0.73$	$4.89 \pm 0.19$

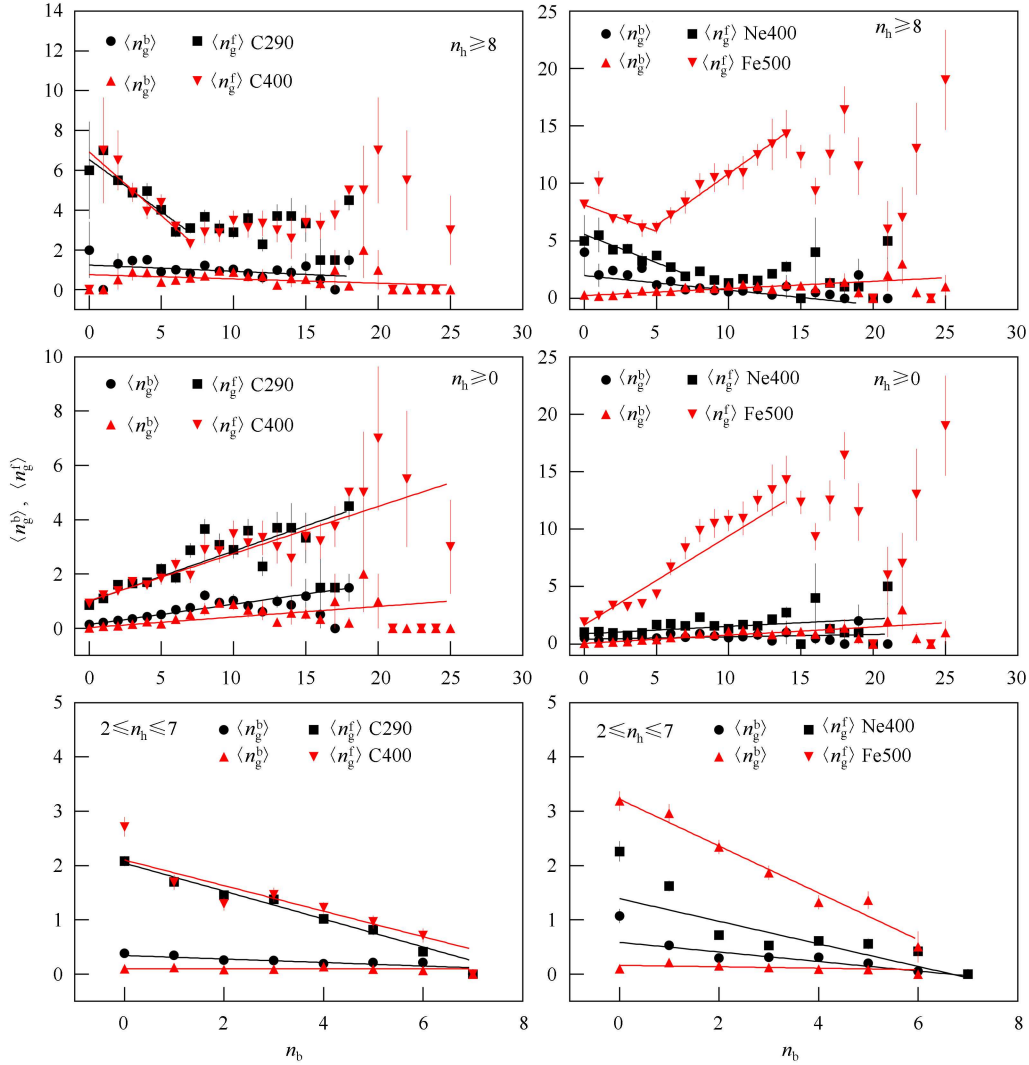


Fig. 2. (color online) Correlations between the averaged multiplicity of backward and forward grey track particles and the number of black track particles for different types of interactions.

Table 3. The fitting parameters of forward-backward multiplicity correlations for nucleus-emulsion interactions with  $2 \leq n_h \leq 7$  using linear relation Eq. (1).

correlation	290 A MeV $^{12}\text{C}$		400 A MeV $^{12}\text{C}$		400 A MeV $^{20}\text{Ne}$		500 A MeV $^{56}\text{Fe}$	
	a	b	a	b	a	b	a	b
$\langle n_b^b \rangle - n_b$	-0.032±0.011	0.342±0.035	0.0003±0.010	0.097±0.034	-0.088±0.012	0.583±0.045	-0.013±0.011	0.161±0.029
$\langle n_b^{fg} \rangle - n_b$	-0.257±0.017	2.043±0.060	-0.235±0.027	2.101±0.101	-0.208±0.022	1.389±0.076	-0.431±0.036	3.221±0.117
$\langle n_b^f \rangle - n_g$	-0.105±0.016	0.845±0.037	-0.123±0.033	1.151±0.069	-0.148±0.020	1.116±0.048	-0.105±0.018	0.956±0.058
$\langle n_b^{fg} \rangle - n_g$	-0.246±0.023	2.318±0.057	-0.187±0.040	2.221±0.082	-0.302±0.023	2.301±0.057	-0.229±0.022	1.967±0.080
$\langle n_b^f \rangle - n_h$	0.062±0.011	-0.012±0.042	0.034±0.008	-0.058±0.029	0.129±0.016	-0.122±0.053	0.040±0.008	-0.044±0.030
$\langle n_b^{fg} \rangle - n_h$	0.301±0.019	0.102±0.074	0.343±0.027	-0.129±0.113	0.274±0.026	-0.158±0.086	0.544±0.028	-0.128±0.115
$\langle n_b^f \rangle - n_h$	0.178±0.012	-0.078±0.047	0.226±0.027	-0.027±0.085	0.231±0.022	0.040±0.078	0.137±0.017	0.061±0.071
$\langle n_b^{fg} \rangle - n_h$	0.455±0.018	-0.020±0.072	0.397±0.021	0.199±0.111	0.365±0.028	0.234±0.098	0.277±0.024	0.121±0.100
$\langle n_b^f \rangle - n_b^b$	-0.012±0.048	0.191±0.054	-0.027±0.059	1.973±0.087	0.004±0.051	1.622±0.068	0.022±0.060	1.365±0.065
$\langle n_b^{fg} \rangle - n_b^b$	-0.069±0.019	0.306±0.027	0.001±0.018	0.092±0.024	-0.091±0.024	0.455±0.039	-0.018±0.020	0.145±0.019
$\langle n_b^f \rangle - n_b^b$	0.022±0.059	-0.011±0.073	0.080±0.074	-0.052±0.125	0.051±0.031	-0.036±0.071	0.025±0.142	-0.005±0.177
$\langle n_b^{fg} \rangle - n_b^b$	0.931±0.019	0.306±0.027	1.001±0.019	0.092±0.024	0.909±0.024	0.455±0.039	0.982±0.020	0.145±0.019
$\langle n_b^f \rangle - n_b^f$	-0.267±0.053	3.465±0.063	-0.241±0.066	3.553±0.102	-0.232±0.053	2.751±0.069	-0.429±0.073	4.106±0.096
$\langle n_b^{fg} \rangle - n_b^f$	-0.002±0.018	0.676±0.042	-0.038±0.034	1.038±0.080	0.016±0.030	0.904±0.061	-0.006±0.027	0.696±0.053
$\langle n_b^f \rangle - n_f^b$	-0.017±0.013	0.294±0.030	0.011±0.013	0.079±0.028	-0.107±0.020	0.551±0.047	-0.009±0.013	0.150±0.025
$\langle n_b^{fg} \rangle - n_f^b$	-0.253±0.022	1.859±0.058	-0.199±0.039	1.745±0.101	-0.258±0.025	1.281±0.066	-0.426±0.048	2.939±0.106
$\langle n_b^f \rangle - n_f^b$	-0.037±0.021	1.008±0.049	-0.040±0.036	1.143±0.087	-0.095±0.030	1.475±0.065	-0.024±0.029	0.855±0.060
$\langle n_b^{fg} \rangle - n_f^b$	0.747±0.022	1.859±0.058	0.801±0.039	1.745±0.101	0.743±0.025	1.279±0.066	0.574±0.048	2.939±0.106
$\langle n_b^f \rangle - n_b^f$	-0.072±0.064	1.390±0.039	0.095±0.194	1.352±0.060	0.290±0.064	0.776±0.039	0.415±0.160	2.285±0.079
$\langle n_b^{fg} \rangle - n_b^f$	-0.141±0.041	0.718±0.029	-0.001±0.158	0.980±0.050	-0.199±0.051	0.996±0.039	-0.040±0.108	0.700±0.040
$\langle n_b^f \rangle - n_g^b$	-0.099±0.067	1.938±0.039	0.058±0.184	1.940±0.060	-0.344±0.059	1.748±0.057	-0.172±0.124	1.406±0.050
$\langle n_b^{fg} \rangle - n_g^b$	0.859±0.041	0.718±0.029	0.978±0.155	0.981±0.050	0.795±0.052	0.998±0.039	0.960±0.108	0.700±0.040
$\langle n_b^f \rangle - n_g^f$	-0.193±0.088	3.331±0.049	0.180±0.215	3.291±0.070	-0.080±0.074	2.559±0.058	-0.060±0.206	3.720±0.080
$\langle n_b^{fg} \rangle - n_g^f$	-0.008±0.014	0.271±0.028	0.001±0.011	0.094±0.018	0.117±0.025	0.271±0.028	0.003±0.009	0.124±0.025
$\langle n_b^f \rangle - n_g^f$	-0.103±0.017	0.823±0.036	-0.120±0.036	1.141±0.071	-0.184±0.025	1.085±0.048	-0.109±0.018	0.951±0.058
$\langle n_b^{fg} \rangle - n_g^f$	-0.249±0.026	2.252±0.053	-0.212±0.041	2.229±0.077	-0.366±0.031	1.958±0.058	-0.240±0.022	1.942±0.078
$\langle n_b^f \rangle - n_h^f$	-0.109±0.021	1.080±0.041	-0.144±0.033	1.263±0.071	-0.058±0.028	1.354±0.052	-0.106±0.020	1.077±0.065
$\langle n_b^{fg} \rangle - n_h^f$	0.751±0.026	2.253±0.053	0.788±0.041	2.229±0.077	0.634±0.031	1.958±0.058	0.760±0.022	1.942±0.078

Table 4. The fitting parameters of forward-backward multiplicity correlations for nucleus-emulsion interactions with  $n_h \geq 8$  using linear relation Eq. (1).

correlation	290 A MeV $^{12}\text{C}$		400 A MeV $^{12}\text{C}$		400 A MeV $^{20}\text{Ne}$		500 A MeV $^{56}\text{Fe}$	
	a	b	a	b	a	b	a	b
$\langle n_b^b \rangle - n_b$	-0.031±0.016	1.241±0.138	-0.021±0.012	0.760±0.126	-0.127±0.017	1.972±0.155	0.062±0.007	0.220±0.051
$\langle n_b^{fg} \rangle - n_b$	-0.526±0.069	6.543±0.346	-0.641±0.105	6.928±0.603	-0.493±0.075	5.560±0.408	-0.460±0.104	8.117±0.894
$\langle n_b^f \rangle - n_g$	-0.089±0.024	2.672±0.134	0.009±0.044	3.034±0.199	-0.266±0.036	3.526±0.154	-0.304±0.073	3.238±0.358
$\langle n_b^{fg} \rangle - n_g$	-0.208±0.043	6.271±0.229	-0.160±0.052	6.814±0.292	-0.476±0.052	6.710±0.236	-0.413±0.096	5.862±0.428
$\langle n_b^f \rangle - n_h$	0.096±0.011	-0.176±0.134	0.016±0.011	0.300±0.144	-0.015±0.022	1.175±0.259	0.044±0.004	-0.069±0.068
$\langle n_b^{fg} \rangle - n_h$	0.345±0.020	-0.538±0.268	0.197±0.021	0.768±0.305	0.136±0.035	0.807±0.394	0.595±0.011	-1.008±0.199
$\langle n_b^f \rangle - n_h$	0.157±0.015	0.310±0.197	0.232±0.016	-0.062±0.227	0.259±0.025	-0.221±0.291	0.083±0.006	0.647±0.104
$\langle n_b^{fg} \rangle - n_h$	0.481±0.027	-0.479±0.313	0.483±0.022	-0.261±0.315	0.644±0.031	-2.081±0.348	0.266±0.010	0.363±0.165
$\langle n_b^f \rangle - n_b^b$	0.331±0.080	4.614±0.218	0.093±0.005	4.583±0.313	0.368±0.105	4.171±0.287	0.817±0.075	3.428±0.206
$\langle n_b^{fg} \rangle - n_b^b$	-0.092±0.033	1.198±0.098	-0.015±0.030	0.668±0.114	-0.222±0.038	1.643±0.132	0.123±0.022	0.482±0.061
$\langle n_b^f \rangle - n_b^f$	0.250±0.115	-0.441±0.363	0.188±0.136	-0.318±0.494	0.168±0.112	-0.303±0.378	0.045±0.295	-0.015±0.708
$\langle n_b^{fg} \rangle - n_b^f$	0.900±0.034	1.215±0.100	0.984±0.030	0.668±0.114	0.774±0.039	1.654±0.132	1.123±0.022	0.483±0.061
$\langle n_b^f \rangle - n_b^f$	0.120±0.097	8.677±0.239	0.517±0.111	0.0002±0.309	-0.028±0.117	7.604±0.302	1.302±0.164	11.444±0.437
$\langle n_b^{fg} \rangle - n_b^f$	0.098±0.025	1.737±0.151	0.205±0.028	1.828±0.193	0.128±0.031	1.933±0.186	0.182±0.016	1.122±0.098
$\langle n_b^f \rangle - n_f^b$	-0.042±0.018	1.227±0.117	-0.031±0.017	0.769±0.124	-0.132±0.022	1.639±0.142	0.068±0.010	0.320±0.054
$\langle n_b^{fg} \rangle - n_f^b$	-0.198±0.027	4.640±0.194	-0.052±0.037	3.651±0.241	-0.220±0.036	3.501±0.221	0.345±0.043	6.828±0.204
$\langle n_b^f \rangle - n_f^b$	0.057±0.026	2.977±0.158	0.203±0.021	2.481±0.177	0.045±0.029	3.501±0.188	0.232±0.017	1.518±0.115
$\langle n_b^{fg} \rangle - n_f^b$	0.803±0.028	4.634±0.197	0.942±0.038	3.680±0.246	0.762±0.037	3.584±0.224	1.349±0.044	6.820±0.206
$\langle n_b^f \rangle - n_g^b$	0.419±0.065	3.148±0.125	0.537±0.111	3.206±0.151	0.318±0.100	2.082±0.129	1.681±0.254	7.900±0.264
$\langle n_b^{fg} \rangle - n_g^b$	-0.173±0.049	2.447±0.099	0.105±0.099	3.062±0.136	-0.436±0.067	3.106±0.121	0.334±0.074	1.948±0.084
$\langle n_b^f \rangle - n_g^f$	-0.185±0.112	5.563±0.172	-0.299±0.214	6.435±0.267	-0.743±0.139	5.895±0.214	0.968±0.146	4.570±0.177
$\langle n_b^{fg} \rangle - n_g^f$	0.827±0.049	2.447±0.098	1.105±0.099	3.062±0.136	0.564±0.067	3.106±0.121	1.334±0.075	1.948±0.084
$\langle n_b^f \rangle - n_h^b$	0.203±0.143	8.741±0.187	-0.052±0.265	9.641±0.291	-0.486±0.162	8.021±0.234	2.774±0.312	12.414±0.358
$\langle n_b^{fg} \rangle - n_h^b$	0.091±0.024	0.671±0.094	0.034±0.034	0.503±0.115	0.119±0.031	0.764±0.099	0.060±0.010	0.197±0.077
$\langle n_b^f \rangle - n_h^f$	-0.120±0.032	2.679±0.133	-0.023±0.059	3.109±0.216	-0.219±0.049	3.133±0.143	0.055±0.015	1.672±0.133
$\langle n_b^{fg} \rangle - n_h^f$	-0.231±0.056	6.239±0.226	-0.102±0.098	6.581±0.330	-0.250±0.059	5.814±0.218	0.256±0.027	3.104±0.233
$\langle n_b^f \rangle - n_h^f$	-0.037±0.040	3.412±0.149	0.001±0.066	3.652±0.234	-0.121±0.046	3.968±0.147	0.117±0.018	1.882±0.157
$\langle n_b^{fg} \rangle - n_h^f$	0.763±0.057	6.257±0.229	0.904±0.103	6.586±0.337	0.809±0.063	5.704±0.222	1.256±0.027	3.104±0.233

Table 5. The fitting parameters of forward-backward multiplicity correlations for nucleus-emulsion interactions with  $n_h \geq 0$  using linear relation Eq. (1).

correlation	290 A MeV $^{12}\text{C}$		400 A MeV $^{12}\text{C}$		400 A MeV $^{20}\text{Ne}$		500 A MeV $^{56}\text{Fe}$	
	a	b	a	b	a	b	a	b
$\langle n_b \rangle - n_b$	0.075±0.006	0.135±0.016	0.039±0.004	0.025±0.009	0.021±0.007	0.416±0.036	0.072±0.005	0.049±0.014
$\langle n_b \rangle - n_b$	0.186±0.011	0.988±0.043	0.174±0.015	1.012±0.072	0.065±0.011	0.882±0.058	0.766±0.038	1.654±0.115
$\langle n_g \rangle - n_g$	0.172±0.013	0.577±0.032	0.290±0.027	0.864±0.063	0.117±0.020	1.005±0.044	0.159±0.009	0.440±0.036
$\langle n_g \rangle - n_g$	0.383±0.023	1.578±0.056	0.459±0.034	1.938±0.109	0.186±0.032	1.875±0.071	0.395±0.014	0.855±0.060
$\langle n_h \rangle - n_h$	0.079±0.003	-0.048±0.011	0.040±0.004	-0.073±0.020	0.085±0.006	0.009±0.024	0.040±0.002	-0.023±0.009
$\langle n_h \rangle - n_h$	0.301±0.007	0.097±0.028	0.235±0.009	0.289±0.051	0.226±0.009	-0.074±0.030	0.557±0.006	-0.185±0.035
$\langle n_h \rangle - n_h$	0.182±0.005	-0.080±0.019	0.232±0.007	-0.061±0.038	0.237±0.008	0.027±0.036	0.109±0.003	0.121±0.024
$\langle n_h \rangle - n_h$	0.445±0.007	0.006±0.029	0.470±0.008	-0.013±0.047	0.458±0.010	-0.023±0.043	0.277±0.005	0.142±0.034
$\langle n_h \rangle - n_h$	1.011±0.043	1.461±0.047	1.052±0.058	1.449±0.091	0.798±0.053	1.320±0.064	1.233±0.051	1.267±0.065
$\langle n_h \rangle - n_h$	0.129±0.016	0.261±0.018	0.094±0.014	0.102±0.019	0.037±0.018	0.455±0.032	0.180±0.015	0.151±0.018
$\langle n_h \rangle - n_h$	0.089±0.054	0.030±0.054	0.085±0.065	0.045±0.102	0.061±0.047	-0.041±0.076	0.030±0.174	-0.007±0.185
$\langle n_h \rangle - n_h$	1.129±0.016	0.261±0.018	1.094±0.014	0.102±0.019	1.036±0.018	0.455±0.032	1.180±0.015	0.151±0.018
$\langle n_h \rangle - n_h$	1.463±0.061	2.713±0.074	1.465±0.079	2.693±0.131	0.953±0.067	2.299±0.089	2.787±0.122	4.105±0.173
$\langle n_h \rangle - n_h$	0.262±0.011	0.293±0.024	0.343±0.015	0.434±0.045	0.276±0.016	0.593±0.040	0.260±0.011	0.411±0.031
$\langle n_h \rangle - n_h$	0.088±0.008	0.164±0.017	0.058±0.007	0.038±0.015	0.025±0.011	0.429±0.035	0.088±0.007	0.082±0.016
$\langle n_h \rangle - n_h$	0.192±0.014	1.119±0.044	0.235±0.021	1.088±0.071	0.095±0.019	0.928±0.058	0.813±0.036	2.097±0.101
$\langle n_h \rangle - n_h$	0.346±0.013	0.464±0.031	0.383±0.012	0.499±0.045	0.321±0.016	1.013±0.049	0.329±0.011	0.507±0.032
$\langle n_h \rangle - n_h$	1.201±0.015	1.107±0.044	1.239±0.021	1.081±0.071	1.095±0.019	0.928±0.058	1.827±0.037	2.081±0.101
$\langle n_h \rangle - n_h$	0.816±0.049	1.356±0.039	1.010±0.091	1.610±0.068	0.619±0.060	0.846±0.039	3.300±0.219	3.602±0.128
$\langle n_h \rangle - n_h$	0.300±0.035	0.898±0.029	0.718±0.082	1.332±0.059	0.079±0.044	1.211±0.047	0.714±0.062	0.954±0.039
$\langle n_h \rangle - n_h$	0.937±0.078	2.053±0.058	1.345±0.165	2.748±0.108	0.293±0.085	2.190±0.077	1.890±0.123	2.117±0.079
$\langle n_h \rangle - n_h$	1.300±0.035	0.808±0.029	1.718±0.082	1.332±0.059	1.079±0.044	1.211±0.047	1.714±0.062	0.954±0.039
$\langle n_h \rangle - n_h$	1.760±0.114	3.400±0.078	2.275±0.224	4.370±0.147	0.910±0.114	3.040±0.097	5.244±0.274	5.717±0.187
$\langle n_h \rangle - n_h$	0.126±0.011	0.161±0.016	0.089±0.013	0.087±0.019	0.199±0.018	0.271±0.027	0.068±0.005	0.045±0.017
$\langle n_h \rangle - n_h$	0.200±0.017	0.600±0.033	0.306±0.034	0.941±0.070	0.167±0.029	1.038±0.046	0.150±0.009	0.505±0.037
$\langle n_h \rangle - n_h$	0.449±0.031	1.664±0.058	0.628±0.061	1.913±0.121	0.332±0.040	1.911±0.072	0.412±0.016	0.904±0.062
$\langle n_h \rangle - n_h$	0.343±0.022	0.746±0.040	0.400±0.038	1.033±0.075	0.339±0.030	1.336±0.053	0.221±0.010	0.549±0.043
$\langle n_h \rangle - n_h$	1.452±0.031	1.661±0.059	1.648±0.063	1.892±0.121	1.381±0.042	1.884±0.072	1.412±0.016	0.904±0.062

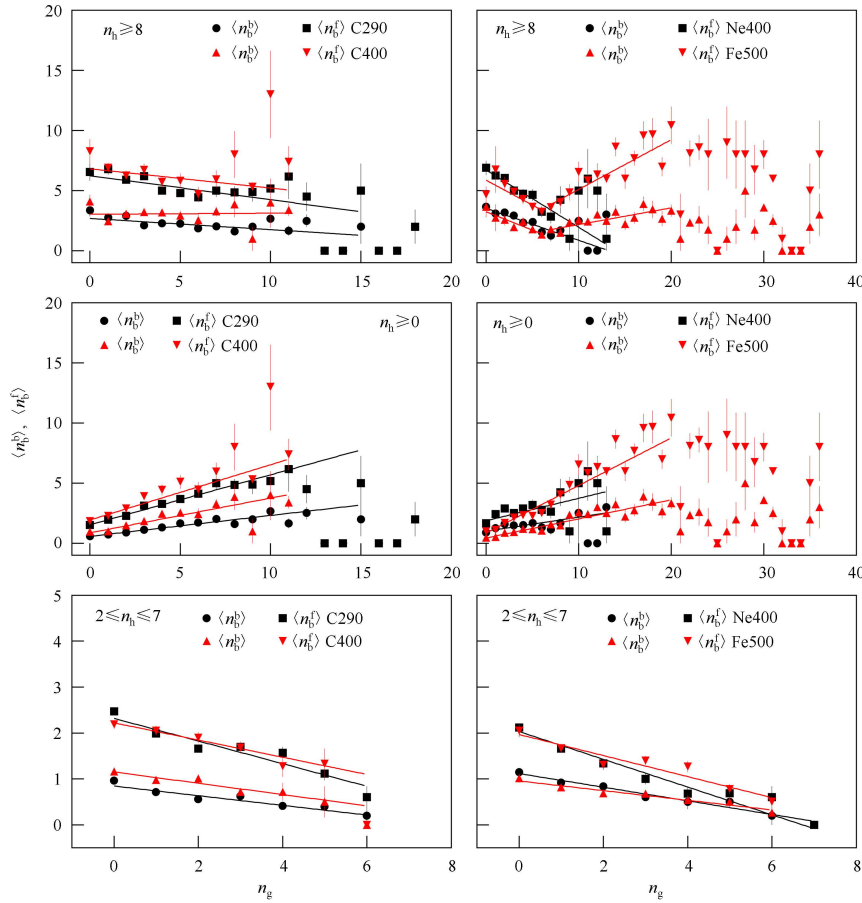


Fig. 3. (color online) Correlations between the averaged multiplicity of backward and forward black track particles and the number of grey track particles for different types of interactions.

Figure 3 shows the correlation between  $\langle n_b^b \rangle$ ,  $\langle n_b^f \rangle$  and  $n_g$  for 290 A MeV  $^{12}\text{C}$ , 400 A MeV  $^{12}\text{C}$ , 400 A MeV  $^{20}\text{Ne}$ , and 500 A MeV  $^{56}\text{Fe}$  induced different types of emulsion target interactions. It can be seen that for interactions with  $n_h \geq 8$ ,  $\langle n_b^f \rangle$  decreases with the increase of  $n_g$  first and then becomes saturated except for the 500 A MeV  $^{56}\text{Fe}$ -AgBr interaction, where  $\langle n_b^f \rangle$  decreases first and then increases with the increase of  $n_g$ , and finally becomes saturated;  $\langle n_b^b \rangle$  decreases slowly with the increase of  $n_g$  except for 500 A MeV  $^{56}\text{Fe}$ -AgBr interaction where the same tendency occurs as the ones in the correlation of  $\langle n_b^f \rangle$  and  $n_g$ . For interactions with  $2 \leq n_h \leq 7$ ,  $\langle n_b^f \rangle$  decreases with the increase of  $n_b$ , and  $\langle n_b^b \rangle$  decreases slowly with the increase of  $n_g$ . For all the interactions,  $\langle n_b^b \rangle$  increases slowly with the increase of  $n_g$  except for 500 A MeV  $^{56}\text{Fe}$ -emulsion interactions, where  $\langle n_b^b \rangle$  increases first and then becomes saturated with the

increase of  $n_g$ , and  $\langle n_b^f \rangle$  increases with the increase of  $n_g$  first and then becomes saturated. The correlations can be represented by a linear relation which is the same as Eq. (1). The fitted lines are plotted in Fig. 3 and the fitting parameters are presented in Tables 3–5. Some of the fitting parameters are from the first a few data sets.

Figure 4 shows the correlation between  $\langle n_b^b \rangle$ ,  $\langle n_b^f \rangle$ ,  $\langle n_g^b \rangle$ ,  $\langle n_g^f \rangle$  and  $n_h$  for 290 A MeV  $^{12}\text{C}$ , 400 A MeV  $^{12}\text{C}$ , 400 A MeV  $^{20}\text{Ne}$ , and 500 A MeV  $^{56}\text{Fe}$  induced different types of emulsion target interactions. It can be seen that for different types of interactions  $\langle n_b^f \rangle$  and  $\langle n_g^f \rangle$  increases with the increase of  $n_h$ ,  $\langle n_b^b \rangle$  and  $\langle n_g^b \rangle$  increases slowly with the increase of  $n_h$ . The correlations can be represented by a linear relation which is the same as Eq. (1). The fitted lines are shown in Fig. 4 and the fitting parameters are presented in Tables 3–5.

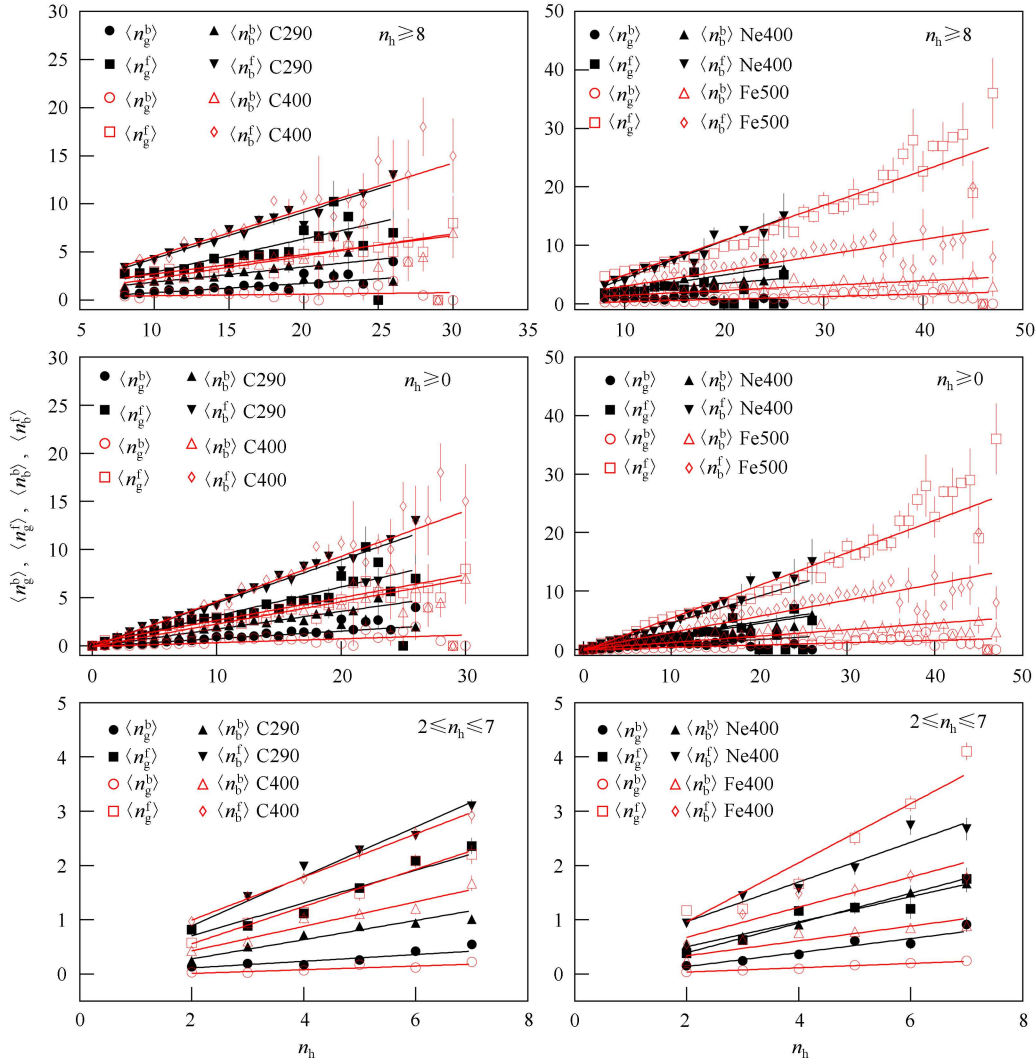


Fig. 4. (color online) Correlations of the averaged multiplicity of backward-forward black and grey track particles with the number of heavily ionized track particles for different types of interactions.

Figure 5 shows the correlation between  $\langle n_b^f \rangle$ ,  $\langle n_g^b \rangle$ ,  $\langle n_g^f \rangle$ ,  $\langle n_h^b \rangle$ ,  $\langle n_h^f \rangle$  and  $n_b^b$  for 290 A MeV  $^{12}\text{C}$ , 400 A MeV  $^{12}\text{C}$ , 400 A MeV  $^{20}\text{Ne}$ , and 500 A MeV  $^{56}\text{Fe}$  induced different type of emulsion target interactions. For interactions with  $2 \leq n_h \leq 7$ ,  $\langle n_h^b \rangle$  and  $\langle n_g^f \rangle$  increases with the increase of  $n_b^b$ ,  $\langle n_g^f \rangle$  and  $\langle n_g^b \rangle$  decreases with the increase of  $n_b^b$  except for the correlation of  $\langle n_g^b \rangle$  and  $n_b^b$  for 400 A MeV  $^{12}\text{C}$  where the correlation is not obvious,  $\langle n_b^f \rangle$  changes slowly with the increase of  $n_b^b$  and the error of the fitted slope parameter is large. For interactions with  $n_h \geq 8$ ,  $\langle n_h^f \rangle$ ,  $\langle n_h^b \rangle$ ,  $\langle n_g^f \rangle$ , and  $\langle n_b^f \rangle$  increase with the increase of  $n_b^b$  except for the correlation of  $\langle n_h^f \rangle$  and  $n_b^b$  in case of 400 A MeV  $^{20}\text{Ne}$  where the correlation is not evident,  $\langle n_g^b \rangle$  decreases with the increase of  $n_b^b$  except for the case of 500 A MeV  $^{56}\text{Fe}$  where  $\langle n_g^b \rangle$  increases with the increase of  $n_b^b$ . For all of the interactions,  $\langle n_b^f \rangle$ ,  $\langle n_g^b \rangle$ ,

$\langle n_g^f \rangle$ ,  $\langle n_h^b \rangle$ , and  $\langle n_h^f \rangle$  increase with the increase of  $n_b^b$ . The correlations can be represented by a linear relation which is the same as Eq. (1). The fitted lines are shown in Fig. 5 and the fitting parameters are presented in Tables 3–5.

Figure 6 shows the correlation between  $\langle n_b^b \rangle$ ,  $\langle n_g^b \rangle$ ,  $\langle n_g^f \rangle$ ,  $\langle n_h^b \rangle$ ,  $\langle n_h^f \rangle$  and  $n_b^f$  for 290 A MeV  $^{12}\text{C}$ , 400 A MeV  $^{12}\text{C}$ , 400 A MeV  $^{20}\text{Ne}$ , and 500 A MeV  $^{56}\text{Fe}$  induced different types of emulsion target interactions. For interactions with  $2 \leq n_h \leq 7$ ,  $\langle n_b^b \rangle$ ,  $\langle n_g^b \rangle$ ,  $\langle n_g^f \rangle$  and  $\langle n_h^b \rangle$  decrease with the increase of  $n_b^f$  except for correlation of  $\langle n_g^b \rangle$  and  $n_b^f$  in the case of 400 A MeV  $^{12}\text{C}$  where the correlation is not obvious (the fitted slope is  $0.011 \pm 0.013$ ) and for correlation of  $\langle n_b^b \rangle$  and  $n_b^f$  in the case of 400 A MeV  $^{20}\text{Ne}$  where the correlation is not evident (the fitted slope is  $0.016 \pm 0.030$ ),  $\langle n_h^f \rangle$  increases with the increase of  $n_b^f$ . For interactions with  $n_h \geq 8$ ,  $\langle n_h^f \rangle$ ,  $\langle n_h^b \rangle$ , and  $\langle n_b^b \rangle$  increase

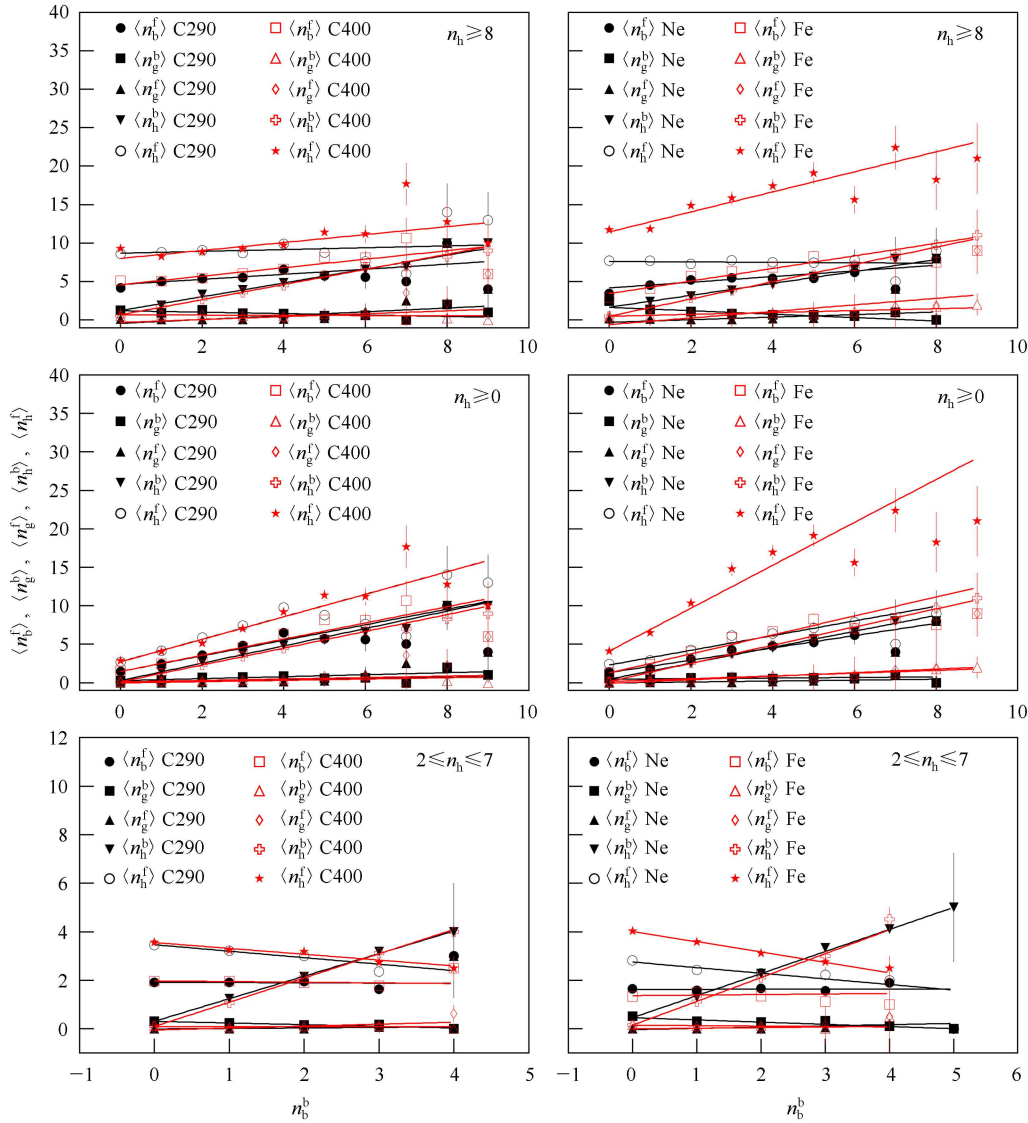


Fig. 5. (color online) Correlations between  $\langle n_b^f \rangle$ ,  $\langle n_g^b \rangle$ ,  $\langle n_g^f \rangle$ ,  $\langle n_h^b \rangle$ , and  $\langle n_h^f \rangle$  and  $n_b^b$  for different types of interactions.

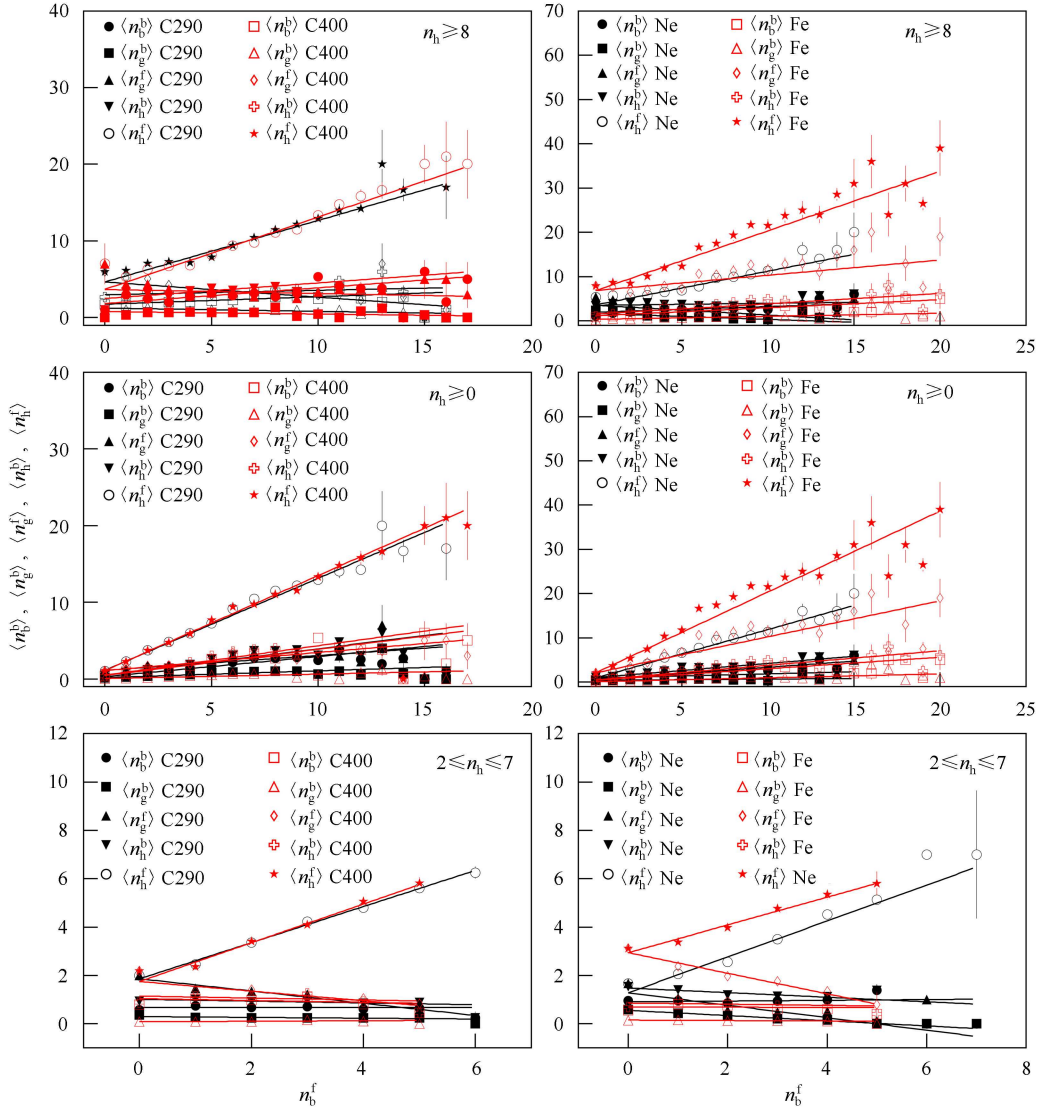


Fig. 6. (color online) Correlations between  $\langle n_b^b \rangle$ ,  $\langle n_g^b \rangle$ ,  $\langle n_h^b \rangle$ , and  $\langle n_b^f \rangle$ ,  $\langle n_g^f \rangle$ , and  $\langle n_h^f \rangle$  for different types of interactions.

with the increase of  $n_b^f$ ,  $\langle n_g^f \rangle$  and  $\langle n_b^b \rangle$  decreases with the increase of  $n_b^f$  except for the case of 500 A MeV  $^{56}\text{Fe}$  where  $\langle n_g^f \rangle$  and  $\langle n_b^b \rangle$  increases with the increase of  $n_b^f$ . For all of the interactions,  $\langle n_b^b \rangle$ ,  $\langle n_g^b \rangle$ ,  $\langle n_h^b \rangle$ , and  $\langle n_b^f \rangle$  increase with the increase of  $n_b^f$ . The correlations can be represented by a linear relation which is the same as Eq. (1). The fitted lines are shown in Fig. 6 and the fitting parameters are presented in Tables 3–5.

Figure 7 shows the correlation between  $\langle n_g^f \rangle$ ,  $\langle n_b^b \rangle$ ,  $\langle n_h^f \rangle$ ,  $\langle n_b^b \rangle$ ,  $\langle n_h^b \rangle$  and  $n_b^b$  for 290 A MeV  $^{12}\text{C}$ , 400 A MeV  $^{12}\text{C}$ , 400 A MeV  $^{20}\text{Ne}$ , and 500 A MeV  $^{56}\text{Fe}$  induced different types of emulsion target interactions. For interactions with  $2 \leq n_h \leq 7$ ,  $\langle n_g^f \rangle$ ,  $\langle n_b^b \rangle$ , and  $\langle n_h^f \rangle$  decrease with the increase of  $n_b^b$  except for the correlation of  $\langle n_h^f \rangle$  and  $n_b^b$  in the case of 400 A MeV  $^{12}\text{C}$  where the correlation is not obvious (the fitted slope is  $0.180 \pm 0.215$ ) and for the correlation of  $\langle n_b^f \rangle$  and  $n_b^b$  in the case of 400 A MeV  $^{20}\text{Ne}$

where the correlation is not evident (the fitted slope is  $0.058 \pm 0.184$ ),  $\langle n_b^b \rangle$  and  $\langle n_g^f \rangle$  increase with the increase of  $n_b^b$  except for the correlation of  $\langle n_g^f \rangle$  and  $n_b^b$  in the case of 290 A MeV  $^{12}\text{C}$  where the error of the fitted slope is large. For interactions with  $n_h \geq 8$ ,  $\langle n_h^f \rangle$ ,  $\langle n_b^b \rangle$ , and  $\langle n_g^f \rangle$  increase with the increase of  $n_b^b$  except for the correlation of  $\langle n_h^f \rangle$  and  $n_b^b$  in the cases of 400 A MeV  $^{20}\text{Ne}$  and 400 A MeV  $^{12}\text{C}$  where the fitted slope is negative,  $\langle n_b^f \rangle$  and  $\langle n_b^b \rangle$  decreases with the increase of  $n_b^b$  except for the case of 500 A MeV  $^{56}\text{Fe}$  where  $\langle n_b^f \rangle$  and  $\langle n_b^b \rangle$  increases with the increase of  $n_b^b$ . For all of the interactions,  $\langle n_g^f \rangle$ ,  $\langle n_b^b \rangle$ ,  $\langle n_h^f \rangle$ , and  $\langle n_h^b \rangle$  increase with the increase of  $n_b^b$ . The correlations can be represented by a linear relation which is the same as Eq. (1). The fitted lines are shown in Fig. 7 and the fitting parameters are presented in Tables 3–5.

Figure 8 shows the correlation between  $\langle n_b^b \rangle$ ,  $\langle n_b^b \rangle$ ,

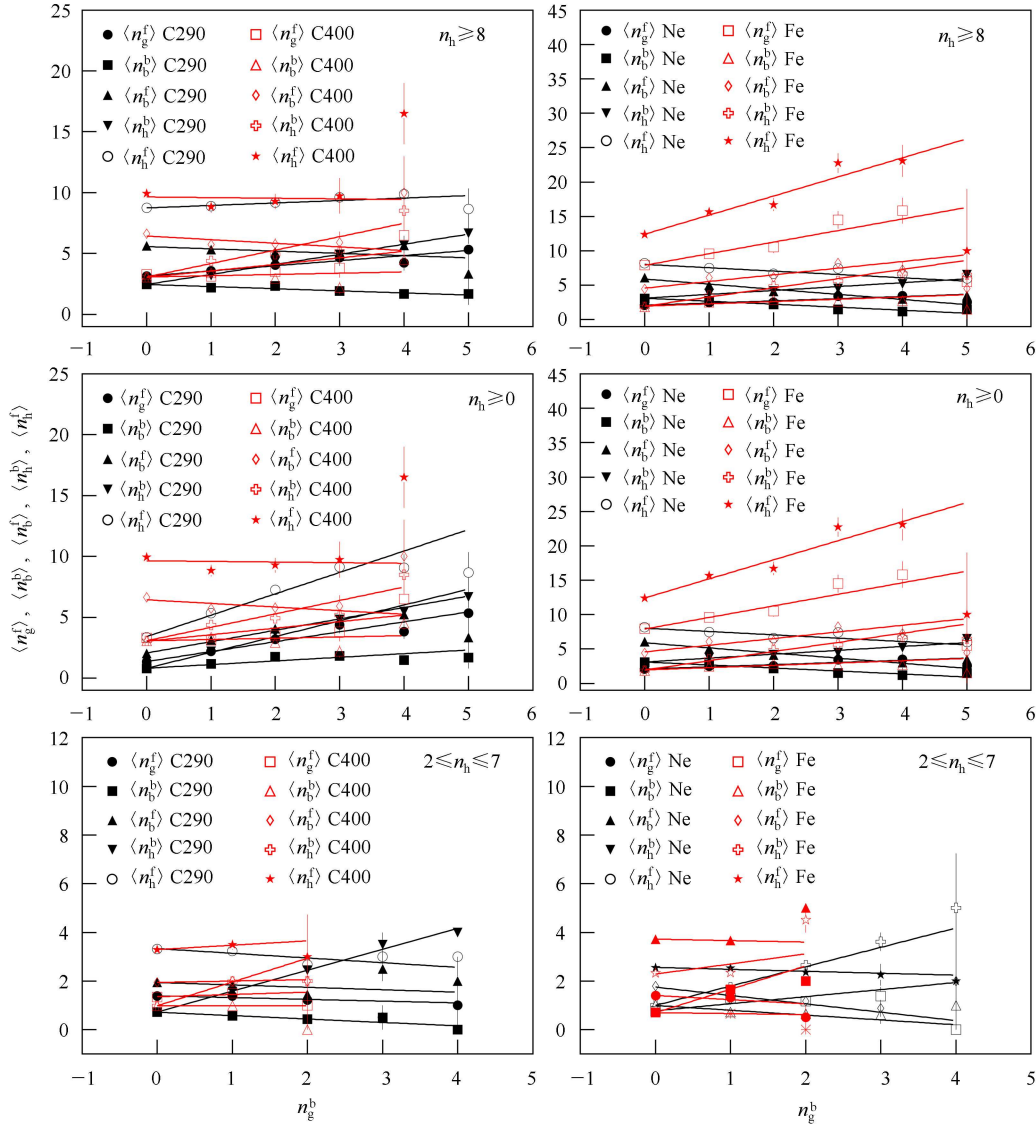


Fig. 7. (color online) Correlations between  $\langle n_g^f \rangle$ ,  $\langle n_b^b \rangle$ ,  $\langle n_h^f \rangle$ ,  $\langle n_h^b \rangle$ , and  $\langle n_h^f \rangle$  and  $n_g^b$  for different types of interactions.

$\langle n_b^f \rangle$ ,  $\langle n_h^b \rangle$ ,  $\langle n_h^f \rangle$  and  $n_g^f$  for 290 A MeV  $^{12}\text{C}$ , 400 A MeV  $^{12}\text{C}$ , 400 A MeV  $^{20}\text{Ne}$ , and 500 A MeV  $^{56}\text{Fe}$  induced different types of emulsion target interactions. For interactions with  $2 \leq n_h \leq 7$ ,  $\langle n_b^b \rangle$ ,  $\langle n_h^b \rangle$ , and  $\langle n_h^f \rangle$  decrease with the increase of  $n_g^f$ ,  $\langle n_b^b \rangle$  and  $\langle n_h^f \rangle$  increase with the increase of  $n_g^f$  except for the correlation of  $\langle n_b^b \rangle$  and  $n_g^f$  in the case of 290 A MeV  $^{12}\text{C}$  where the correlation is not obvious. For interactions with  $n_h \geq 8$ ,  $\langle n_h^f \rangle$  and  $\langle n_b^b \rangle$  increase with the increase of  $n_g^f$ ,  $\langle n_b^b \rangle$ ,  $\langle n_h^b \rangle$ , and  $\langle n_h^f \rangle$  decreases with the increase of  $n_g^f$  except for the case of 500 A MeV  $^{56}\text{Fe}$  where the fitted slope is positive and for the correlation of  $\langle n_b^b \rangle$  and  $n_g^f$  in case of 400 A MeV  $^{12}\text{C}$  where the correlation is not evident. For all the interactions,  $\langle n_b^b \rangle$ ,  $\langle n_h^b \rangle$ ,  $\langle n_h^f \rangle$ ,  $\langle n_h^b \rangle$ , and  $\langle n_h^f \rangle$  increase with the increase of  $n_g^f$ . The correlations can be represented by a linear relation which is the same as Eq. (1). The fitted

lines are shown in Fig. 8 and the fitting parameters are presented in Tables 3–5.

Based on the geometrical picture (the participant-spectator model) [21] and the cascade evaporation model [20] of high energy nucleus-nucleus collisions, the grey track particles are emitted from the target nucleus very soon after the moment of impact, which are the target recoiled protons of energy ranging up to 400 MeV, the black track particles are the images of target evaporated particles of low-energy ( $E < 30$  MeV) and singly or multiply charged fragments. For interactions with  $2 \leq n_h \leq 7$  (nucleus-CNO interactions),  $\langle n_b^b \rangle$  and  $\langle n_h^f \rangle$  decrease with increase of  $n_b$ ,  $\langle n_b^b \rangle$  and  $\langle n_h^f \rangle$  also decrease with increase of  $n_g$  because of the limited target size (the maximum target fragments  $n_h = 8$  which corresponds to the total disintegration of the oxygen nucleus). For interactions

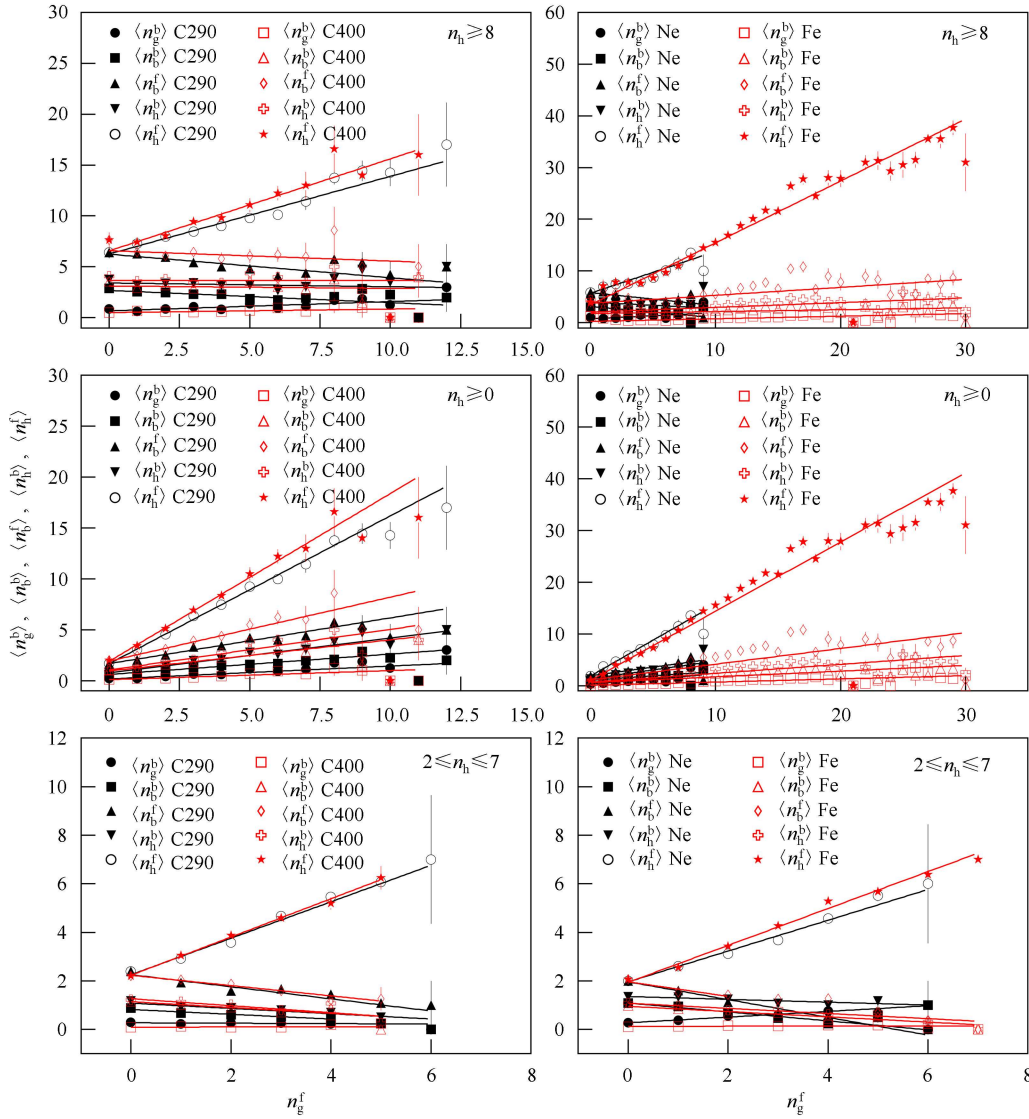


Fig. 8. (color online) Correlations between  $\langle n_g^b \rangle$ ,  $\langle n_b^b \rangle$ ,  $\langle n_g^f \rangle$ ,  $\langle n_b^f \rangle$ , and  $\langle n_h^f \rangle$  and  $n_g^f$  for different types of interactions.

with  $n_h \geq 8$  (nucleus-AgBr interactions) and the light projectile (less than  $^{20}\text{Ne}$ )  $\langle n_g^b \rangle$  decreases with the increase of  $n_b$ , and  $\langle n_g^f \rangle$  decreases first and then remains constant with the increase of  $n_b$  because the minimum target fragments are  $n_h = 8$  and the excitation energy of the target residues increases with the increase of the number of cascading collisions but it is limited for a limited projectile. For interactions with  $n_h \geq 8$  and heavy projectile ( $^{56}\text{Fe}$  projectile), with the increase of  $n_b$  the excitation energy of the target residues and the number of cascading collisions is increased,  $\langle n_g^f \rangle$  decreases first and then increases with the increase of  $n_b$  and finally becomes saturated because of the limited target size. Because of the limitation of the nuclear emulsion detector, we cannot discriminate peripheral or semi-central AgBr target interactions ( $n_h \leq 7$ ) with H and CNO target interactions, this type

of the interaction is classified into the interactions with H target and CNO target interactions. That is why  $\langle n_g^f \rangle$  decreases first with the increase of  $n_b$  for the interaction of  $^{56}\text{Fe}$ -AgBr with  $n_h \geq 8$ . The same mechanism can be used to explain the correlations of  $\langle n_b^b \rangle$ ,  $\langle n_b^f \rangle$  and  $n_g$  for interactions with  $n_h \geq 8$ . For all of the interactions with the increase of  $n_b$  the averaged excitation energy of target residues and the cascading collision in the target spectator increased,  $\langle n_g^b \rangle$  and  $\langle n_g^f \rangle$  will increase but due to the limited target size  $\langle n_g^f \rangle$  finally becomes saturated,  $\langle n_b^b \rangle$  and  $\langle n_b^f \rangle$  increase with increase of  $n_g$  and for interactions of 500 A MeV  $^{56}\text{Fe}$ -emulsion which become saturated when  $n_g$  is greater than 20. With the increase of  $n_h$  the excitation energy of the target residues and the number of cascading collisions increased, so  $\langle n_b^b \rangle$ ,  $\langle n_b^f \rangle$ ,  $\langle n_g^b \rangle$ , and  $\langle n_g^f \rangle$  will increase with the increase of  $n_h$ .

The backward-forward multiplicity correlations can also be explained based on the geometrical picture [21] and the cascade evaporation model [20] of high energy nucleus-nucleus collisions. Generally speaking, with the increase of the grey track particle, the probability of the backward emitted protons and the pions is increased, and with the increase of the black track particle, the probability of the backward emitted target evaporated fragments is increased. For the interactions with  $2 \leq n_h \leq 7$ , with the increase of  $n_b^b$  the excitation energy of the target residues and the cascading collision in the target spectator increased,  $\langle n_h^b \rangle$  and  $\langle n_g^f \rangle$  increased, but  $\langle n_h^f \rangle$ ,  $\langle n_g^b \rangle$ , and  $\langle n_b^f \rangle$  decreased because of the limited target spectators. For the same reasons with the increase of  $n_b^f$ ,  $\langle n_h^f \rangle$  increased but  $\langle n_h^b \rangle$ ,  $\langle n_g^b \rangle$ ,  $\langle n_b^b \rangle$ , and  $\langle n_b^f \rangle$  decreased. With the increase of  $n_g^b$ ,  $\langle n_h^b \rangle$  and  $\langle n_g^f \rangle$  increased, but  $\langle n_h^f \rangle$ ,  $\langle n_g^b \rangle$ , and  $\langle n_b^f \rangle$  decreased. With the increase of  $n_g^f$ ,  $\langle n_b^b \rangle$  and  $\langle n_b^f \rangle$  increased but  $\langle n_h^b \rangle$ ,  $\langle n_b^b \rangle$ , and  $\langle n_b^f \rangle$  decreased. For interactions with  $n_h \geq 8$  and light projectile (less than  $^{20}\text{Ne}$ ), with the increase of  $n_b^b$ ,  $\langle n_g^b \rangle$  decreased but  $\langle n_h^f \rangle$ ,  $\langle n_b^b \rangle$ ,  $\langle n_g^f \rangle$  and  $\langle n_b^f \rangle$  increased; with the increase of  $n_b^f$ ,  $\langle n_g^f \rangle$  and  $\langle n_b^b \rangle$  decreased but  $\langle n_h^b \rangle$ ,  $\langle n_h^f \rangle$ , and  $\langle n_b^b \rangle$  increased; with the increase of  $n_g^b$ ,  $\langle n_b^f \rangle$  and  $\langle n_b^b \rangle$  decreased but  $\langle n_h^f \rangle$ ,  $\langle n_b^b \rangle$ , and  $\langle n_g^f \rangle$  increased; with the increase of  $n_g^f$ ,  $\langle n_b^f \rangle$ ,  $\langle n_b^b \rangle$ , and  $\langle n_h^b \rangle$  decreased but  $\langle n_h^f \rangle$  and  $\langle n_b^b \rangle$  increased. For interactions with  $n_h \geq 8$  and heavy projectile ( $^{56}\text{Fe}$ ), the slopes of all of the backward-forward multiplicity correlations are positive because the number of cascading collisions is greater and the excitation energy of the target residues is greater. For all the interactions the slopes of

all of the backward-forward multiplicity correlations are positive.

## 4 Conclusions

The forward-backward multiplicity and correlations of black track particles and grey track particles emitted in 150 A MeV  $^4\text{He}$ , 290 A MeV  $^{12}\text{C}$ , 400 A MeV  $^{12}\text{C}$ , 400 A MeV  $^{20}\text{Ne}$ , and 500 A MeV  $^{56}\text{Fe}$  induced different types of emulsion target interactions are investigated. It is found that the forward and backward averaged multiplicity of grey, black and heavily ionized track particles increase with the increase of target size. The averaged multiplicity of a forward black track particle, backward black track particle, and backward grey track particle do not depend on the projectile size and energy, but the averaged multiplicity of the forward grey track particle increases with the increase of projectile size and energy. The backward grey track particle multiplicity distribution follows an exponential decay law and the decay constant decreases with an increase of target size. The general characteristics of backward-forward multiplicity correlations of black, grey and heavily ionized track particles are discussed, which can be well explained by the geometrical picture and the cascade evaporation model of high energy nucleus-nucleus collisions.

*We are grateful to Dr N. Yasuda and staff of HIMAC NIRS, Japan for helping to expose nuclear emulsion.*

## References

- 1 Andronenko M N, Volnin E N, Vorobev A A et al. JETP Lett., 1983, **37**: 530–534
- 2 Gavrishchuk O P, Moroz N S, Peresedov V P et al. Nucl. Phys. A, 1991, **523**: 589–596
- 3 Aliev Sh M, Edgorov S O, Lutpullaev S L et al. Sov. J. Nucl. Phys., 1990, **51**: 1008–1009
- 4 Bayukov Yu D, Efremenko V I, Frankel S et al. Phys. Rev. C, 1979, **20**: 764–772
- 5 Angelov N et al. (Bucharest-Dubna-Moscow-Sofiya-Tashkent-Tbilisi-Ulan Bator Collaboration). Sov. J. Nucl. Phys., 1975, **22**: 534
- 6 Agababyan N M et al. (EHS-NA22 collaboration). Z. Phys. C, 1995, **66**: 385–392
- 7 Tufail A, Ahmad S, Zafa M. Can. J. Phys., 1996, **74**: 141–144
- 8 Ghosh D, Roy J, Sengupta R. Nucl. Phys. A, 1987, **470**: 683–691
- 9 Ghosh D, Roy J, Sengupta R. Can. J. Phys., 1989, **67**: 115–118
- 10 Ghosh D, Roy J, Sengupta R, Sarkar Sh. Z. Phys. A, 1992, **342**: 191–193
- 11 Ahmed T, Irfan M. Phys. Rev. C, 1992, **46**: 1483–1486
- 12 El-Nadi M, Abdelsalam A, Moussa N A. Int. J. Mod. Phys. E, 1994, **3**: 811–820
- 13 Namboodiri M N et al. (E802 Collaboration). Nucl. Phys. A, 1994, **566**: 443c–446c
- 14 El-Naghy A, Sadek N M, Mohery M. Nuovo Cimento A, 1997, **110**: 125–133
- 15 Abd Allah N N. Int. J. Mod. Phys. E, 2002, **11**: 105–117
- 16 Abdel-Waged K. J. Phys. G, 1999, **25**: 1721–1732
- 17 Abd Allah N N, Mohery M, Zahran E M, LIU Fu-Hu. Chin. J. Phys., 2004, **42**: 684–693
- 18 ZHANG Dong-Hai, ZHAO Hui-Hua, LIU Fang et al. Chin. Phys., 2006, **15**: 1987–1995
- 19 Baldin A M, Giordenescu N, Ivanova L K et al. Sov. J. Nucl. Phys., 1975, **20**: 629–634
- 20 Powell C F, Fowler P H, Perkins D H. The study of Elementary Particles by the Photographic Method, Pergamon Press. London, New York, Paris, Los Angeles, 1959. 432
- 21 Bowman J D, Swiatecki W J, Tsang C F. Abrasion and ablation of heavy ions. Lawrence Berkeley Report: LBL-2908, 1973